ORIGINAL RESEARCH

Modelling of water absorption kinetics and biocompatibility study of synthesized cellulose nanofiber-assisted starch-graft-poly(acrylic acid) hydrogel nanocomposites

Nooshin Bahadoran Baghbadorani · Tayebeh Behzad · Mohammad Hossein Karimi Darvanjooghi · Nasrin Etesami

Abstract To prepare superabsorbent hydrogels, starch-graft-poly(acrylic acid) reinforced by cellulose nanofibers (CNF), was synthesized through free radical graft polymerization. The results of its biocompatibility tests exhibited that by increasing incubation time from 1 to 5 days, the numbers of living cells were increased on both reinforced and unreinforced hydrogels. However, the fraction of cells on the surfaces of the reinforced hydrogel is comparable to unreinforced samples. The swelling amounts in NaCl, CaCl$_2$, and AlCl$_3$ solutions were 193 ± 9, 110 ± 8, and 99 ± 7 (g$_{water}$/g$_{absorbent}$) for 5 wt% CNF-reinforced hydrogels and 109 ± 8, 62 ± 7, and 56 ± 6 (g$_{water}$/g$_{absorbent}$) for unreinforced hydrogels, respectively. Compressive strength and Young's modulus of 5 wt% CNF-assisted hydrogels were also 63.3 and 31.6 kPa corresponding to 69% and 140% improvements compared with unreinforced one. The graft polymerization of acrylic acid monomer was controlled by monomer content and cross-linking percentage, in order to achieve the highest swelling capacity for hydrogels. Hydrogel swelling in water was 312 g$_{water}$/g$_{absorbent}$ for unreinforced hydrogel and 523 g$_{water}$/g$_{absorbent}$ for 5 wt% CNF-reinforced sample and water absorption kinetics results was in agreement with the pseudo-second-order model. The prepared CNF-reinforced starch-graft-poly(acrylic acid) hydrogels can be used in a wide range of medical application due to the enhanced hydrophilicity, mechanical strength, and biocompatibility.

N. Bahadoran Baghbadorani · T. Behzad (✉) ·
M. H. Karimi Darvanjooghi · N. Etesami
Department of Chemical Engineering, Isfahan University of Technology, Isfahan 84156-83111, Iran
e-mail: tbehzad@cc.iut.ac.ir

Graphic abstract
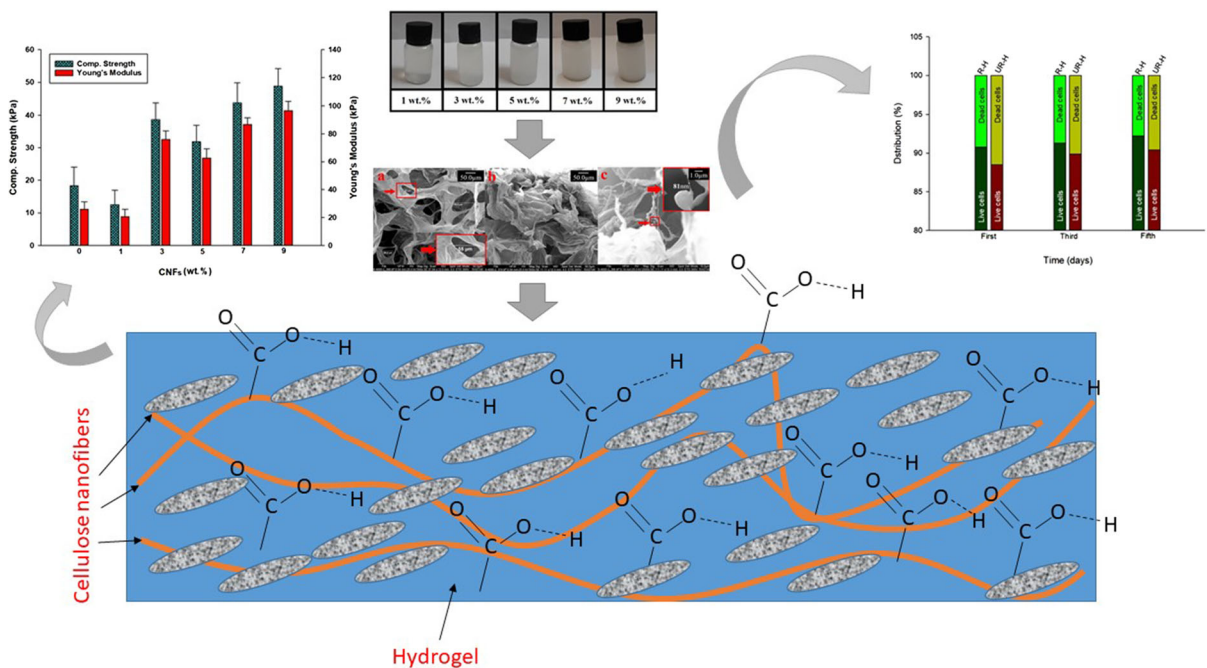
Keywords Starch-graft-poly(acrylic acid) ·
Cellulose nanofibers · Biocompatibility · Hydrogel
Swelling

Introduction

Superabsorbent hydrogels can be classified as novel
materials in the absorption process employed widely
in chemical, biological, and environmental applica-
tions. Current industrial and academic research for
development in superabsorbent hydrogels has been
centered upon inclusion of polysaccharides, i.e.,
starch, chitosan, cellulose, etc. Because of high
biocompatibility and low cost, biodegradability, avail-
ability, and non-toxicity, starch (St) can be selected as
the most suitable material for preparation of hydrogels
(Fajardo et al. 2013; Li et al. 2016; Tanan et al. 2018).

The application of superabsorbent hydrogel can be
determined using three attributes of swelling capacity,
swelling rate, and the strength of swollen hydrogel. It
is mentioned that the quality of these superabsorbents
strongly depends on these factors that can be adjusted
by changing cross-linking density during St-based
hydrogel preparation (Sun et al. 2013). One special

way for the preparation of St-based hydrogel is the
graft-copolymerization of pH-sensitive monomers
including acrylic acid (AA), methacrylic acid
(MAA), and acrylamide (AAm). In fact, the addition
of other chemical functional groups such as carboxylic
acid, sulfonic acid, amine, and hydroxyl to the St
chains, might improve the toughness and strength,
rapid degradation in the presence of other liquids, and
casting process due to the presence of amylopectin
structures (Hoffman 2012; Jayaramudu et al. 2013).

Graft polymerization (denoted as "*g*" in the name
of hydrogels) of St-based hydrogels with Poly(acrylic
acid) (PAA) can be classified as a new hydrogel due to
the higher polarity, more hydrophilicity, and greater
solubility of PAA in comparison with other vinyl
monomers. Thus, they can be employed as a suit-
able substance in various applications ranging from
biomedical practices to agricultural uses. However,
despite their benefits, St-based hydrogels have short-
comings regarding to physical, mechanical, and ther-
mal properties. During the last few years, studies have
been channeled into improving the properties of St-
based hydrogels and preparation of their superab-
sorbent bio-nanocomposites toward, particularly,
medical application (Bakhshi et al. 2016; Ferreira
et al. 2018; Gomes et al. 2015; Pachauri et al. 2017;

Pinheiro et al. 2017; Siqueira et al. 2010; Zander et al. 2014). To do so, isolation of CNF from cellulose, the most abundant biopolymer in nature with linear β-1,4-linked D-glucopyranose units, is in the limelight today. Since hydrogels can be used in biomedical areas, the biocompatibility of CNF plays a vital role besides the reinforcement of hydrogels.

Lately, several studies have been conducted on St-*g*-PAA hydrogels (Aouada et al. 2011; Dai and Kadla 2009; Li et al. 2008; Spagnol et al. 2012a, c; Yue et al. 2016). The mechanical properties of Methyl Cellulose Nanofibers (MCNF)-reinforced polyacrylamide (PAAm) nanocomposite hydrogel was studied under the compressive stress to show the enhancement of maximum compressive stress from 2.1 to 4.4 kPa after incorporation of MCNF (Aouada et al. 2011).

In another study, the swelling capacity and absorption rate of CNF-reinforced chitosan-*g*-PAA hydrogels was considered as another key factors (Spagnol et al. 2012c). Based on the experimental results, the capacity value and the rate constant of the swelling for the hydrogel without CNF were 381 $g_{water}/g_{absorbent}$ and 2.86×10^{-6} min^{-1}, respectively. By adding CNF, these values were increased to 486 $g_{water}/g_{absorbent}$ and 4.06×10^{-6} min^{-1}, respectively. Moreover, it was observed that the water absorption kinetics closely followed the Schott's pseudo-second-order kinetics model, with a correlation coefficient of 0.990. Yue et al. (2016) synthesized CNF-reinforced sodium alginate-poly(vinyl alcohol) hydrogels. The storage modulus and compressive strength of hydrogel with CNF were respectively 13 and 3.2 times of those of neat hydrogels. Li et al. (2008) investigated the mechanical properties of an interpenetrating polymer network (IPN) hydrogel made of the combination of St-*g*-PAA and poly(dimethyl diallyl ammonium chloride). The compressive stress of the St-*g*-PAA hydrogel was found to be 354 kg/m^2, while for the IPN hydrogel, this value was reached to 1398 kg/m^2. Dai and Kadla (2009) investigated the effect of cellulose nanocrystals (CNCs)—as the reinforcement—on the mechanical properties of methylcellulose/hydroxyethyl cellulose hydrogels. They also compared their results with the clay nanoparticle-reinforced counterparts. Based on their findings, Young's modulus of the unreinforced hydrogel was found to be 28 kPa, while this value was increased up to 32 kPa by adding 20 wt% CNCs and decreased to 23 kPa by loading 20 wt% Clay nanoparticles. Spagnol et al. (2012a)

studied the influence of cellulose nanowhiskers (CNWs) on the absorption properties of a complete synthetic poly(acrylamide-*co*-acrylate). The presence of 10 wt% CNWs on the polymeric matrix caused 85% improvement in the absorption value compared to the unreinforced hydrogel.

Other efforts were made on the biocompatibility of the hydrogel-based composites (Deng et al. 2013; Huang et al. 2018; Ye et al. 2016). Ye et al (2016). synthesized St-*g*-poly(sulfobetaine methacrylate) (St-*g*-PSBMA) and performed the toxicity and hemolysis analysis. Their results revealed that the sample had a high degree of biocompatibility and hemocompatibility. Huang et al. (2018) used carboxylated cellulose nanofibril to enhance the reinforcement of poly(AAm-*co*-AA) hydrogel. They observed that the elastic modulus, tensile strength, and toughness of the poly(AAm-*co*-AA) hydrogel were enhanced significantly. Also, the results of biocompatibility tests showed that the nanocomposite hydrogel had no toxicity to the living cells, and they can proliferate its surface, which makes it desirable for tissue engineering applications. Deng et al. (2013) fabricated needle-like nano-hydroxyapatite based on agar-gelatin co-hydrogelation. The biocompatibility of the obtained hydrogel was measured by testing cell proliferation and differentiation of MC3T3-E1 cells. The experimental findings indicated that the hydrogel was significantly favorable for the proliferation of live cells. The biocompatible hydrogel possessed great potential to be implemented as materials for bone tissue engineering.

Cellulose nanofibers can be employed as an interesting biopolymer with extraordinary properties (Wicklein et al. 2015), [aspect ratio of 100–500, the superior strength of 2–6 GPa, elastic modulus of 30–50 GPa (Usov et al. 2015)]. Cellulose nanofibers have two significant advantages in comparison to other typical nano-structured materials such as carbon nanotube and graphene nanosheets. The first point is that cellulose can be found abundantly in natural sources such as wood and non-wood agriculture products such as wheat, cotton, etc. Therefore, this leads to a low cost environmental-friendly and biocompatible material which can be considered in medical applications such as surgery, transplant, and tissue engineering. In addition, due to the active surface of CNF, they can be functionalized by various chemical treatment for specific applications such as

heavy metal removal from environment (Zander et al. 2014).

Accordingly, because hydrogels can be used in wide range of medical applications some important points are needed to be cleared as their essential physico-chemical properties including reinforced quality, biocompatibility, and their ability to absorb water from live tissues. It should be mentioned that CNCs, in combination with CNF have been used in the preparation of chitosan-based hydrogel and no comprehensive study has been carried out on perusing the biocompatibility properties of the bionanocomposite. The novelty of the present work lays on preparation and characterization of CNF reinforced starch-graft-poly(acrylic acid) hydrogels. To do so, the influence of CNF on the absorption kinetics of the synthesized St-g-PAA hydrogels was statistically studied by using a response surface methodology (RSM). Also, the physio-chemical, swelling, mechanical, morphological, and biocompatibility properties of the synthesized St-g-PAA hydrogels were investigated profoundly.

Experimental

Materials

All chemicals (Table 1), used in this research for the preparation of CNF and reinforced hydrogel were of analytical grades and purchased from Merck Chemical Company, Germany.

Table 1 List of chemicals used in this research and their purities

Chemicals	Purity (wt%)
$(C_6H_{10}O_5)_n$-(H_2O)	99.97
Potassium persulfate ($K_2S_2O_8$)	99.99
N,N'-methylene- bisacrylamide (MBA)	99.95
Acrylic acid (AA)	99.60
Sodium hydroxide (NaOH)	99.99
Hydrochloric acid (HCl)	99.99
Hydrogen peroxide (H_2O_2)	99.98
Sodium hypochlorite (NaClO)	99.96

Chemo-mechanical preparation of CNF

To prepare CNF, wheat straw was used as the primary source of cellulose and crushed to very fine particles following the previous work (Jahanbaani et al. 2016). Afterward, 40 mL of NaOH (7.5 w/v%) solution was added to 2 g of the obtained straw particles. Having been under the stirring condition for 2 h, the remaining solid content was rinsed with deionized water several times to set the pH neutral. Then, for the removal of hemicellulose, 40 mL of HCl (2 M) solution was added to the remaining solid, and the mixture was placed in an oven at 75 °C for 135 min. The remaining mixture was again rinsed with deionized water to set pH near to 7, and the obtained pulp was placed in the oven at 60 °C for 48 h to achieve dry solid. The lignin and the remaining hemicellulose were also eliminated from solid cellulose compound by soaking in NaOH (2 wt%) solution at 80 °C for 2 h.

The bleaching process of cellulose fibers was carried out by removing the remaining lignin using H_2O_2 and NaClO. Hence, 0.176 g of pure H_2O_2 was diluted by 40 mL deionized water, and a given amount of NaOH (10 w/v%) solution was added to the solution to increase pH of the solution. The cellulose fibers were then added to this solution, and the mixture was placed in an oven at 50 °C for 1 h. Finally, 0.244 g of NaClO was diluted by 40 mL deionized water and the obtained cellulose fibers were added to this solution. Therefore, a certain amount of H_2SO_4 (1 M) solution was added to the mixture in order to reach pH = 3. The obtained paste was placed in the oven at 50 °C for 48 h to achieve dried cellulose. Chemical components of CNF were measured according to the standard procedures proposed by the National Renewable Energy Laboratory (NREL), (Supplementary information, Table S1) (Sluiter et al. 2008). As it can be observed, the amounts of cellulose, hemicellulose, and lignin were found to be 91.54, 6.47, and 1.99 wt%, respectively. Afterward, the prepared cellulose fibers were disintegrated to nanofibers using Super Grinder device (Masuko Company, model: MKCA-6; Japan). The pulp suspension was passed through the super grinder more than ten times at the rotation speed of 1500 rpm to reduce the dimension of CNF to the nanometer. After preparation of CNF, the resultant nanofibers were soaked into a given amount of water, and the solution was kept under sonication process with cycle time of 0.5 s and the amplitude of

85% for two separate durations of 30 min with 5 min rest between each process. Having been under drying condition for 24 h, the resultant dried CNF were characterized using X-ray diffraction (XRD), Fourier transform infrared (FTIR), and field emission-scanning electron microscopy (FE-SEM).

Optimization of polymerization parameters of St-g-PAA

In order to optimize the polymerization of AA monomers grafted onto the backbone of St, the weight ratio of AA monomers to St (2–5:1, in gram ratio) and the weight percentage of MBA—as the cross-linker—to AA monomer (1–3 wt%) were chosen as the most important variables for the rotatable central composite design (RCCD) by means of RSM, Design-Expert® software version 7.0.0 (Stat-Ease, Inc., Minneapolis, MN, USA). During the optimization, the equilibrium swelling capacity of hydrogels ($g_{water}/g_{absorbent}$) was also calculated as the model response, using the following equation:

$$W_{eq} = \frac{M - M_0}{M_0} \tag{1}$$

Here M and M_0 (g) stand for the swollen and dry weight of hydrogels, and W_{eq} represents the equilibrium swelling capacity of hydrogels ($g_{water}/g_{absorbent}$) (Zohuriaan-Mehr and Pourjavadi 2003). The amount of time, temperature, alkaline hydrolysis, and initiator concentration were selected from the previous studies (Bardajee and Hooshyar 2013; Dai and Kadla 2009; Li et al. 2005; Spagnol et al. 2012a, c). Analysis of variance (ANOVA) was also conducted to determine the optimum conditions (Fig. S1, Table S2).

Preparation of St-based hydrogels

Synthesis of St-g-PAA hydrogels

An adequate amount of St was thoroughly gelatinized in 30 mL water at 85–95 °C for 1 h using a four-necked round-bottom flask, equipped with a condenser, a mechanical homogenizer. Nitrogen gas was then flowed through the flask for a while until the temperature was reached 60 °C. Afterward, 1 wt% potassium persulfate (respect to the weight of AA monomer)—as the initiator—was added to the system. After 10 min, an aqueous solution containing 10 mL

deionized water, 1–3 wt% MBA, and 2–5 g AA monomer were gradually poured into the flask to polymerize the AA monomer on the surface of St molecule chains through radical polymerization. This reaction was continued at 70 °C for 3 h. It is also worth noting that the applied values were chosen based on the boundaries proposed by the software, which were respectively 1.38, 2, 3.5, 5, and 5.62 g for the monomer content and 0.59, 1, 2, 3, and 3.41 wt% for the cross-linking agent percentages. The prepared hydrogels were then completely immersed into an alkaline solution containing sodium hydroxide (2 M) at 90–95 °C for 2 h. This treatment not only could neutralize unreacted carboxyl groups but also, could impart more ionic strength and swelling capacity to the hydrogels (Chen and Tan 2006; Li et al. 2005). In the next step, the ensuing hydrogels were successively solvent-exchanged in order to wash all unreacted chemicals in the reactions. To do so, they were first dipped into ethanol for 2 h to have water replaced with ethanol, then they were cut into small pieces with equal sizes and shapes and swollen again by plunging them into distilled water overnight. Afterward, they were again steeped in ethanol for 24 h to extract all unreacted monomers and water molecules. Finally, the resultant hydrogels were oven-dried at 70 °C for 48 h to reach a constant weight; further drying continued with a freeze-dryer at − 55 °C for 48 h (Bardajee and Hooshyar 2013; Li et al. 2005).

Synthesis of CNF-reinforced hydrogels

After optimizing the required amount of AA monomer (3.65 g) and cross-linking agent (1.12 wt%) based on the equilibrium swelling capacity of hydrogels using Design-Expert software, the same procedure was employed in order to prepare hydrogels reinforced with different concentrations of CNF (1, 3, 5, 7, and 9 wt%, which their suspension images are shown in Fig. 1). Hence, CNF were simultaneously added into the flask, together with the monomer, cross-linking agent, and deionized water (Spagnol et al. 2012a, c).

Characterization

XRD analysis

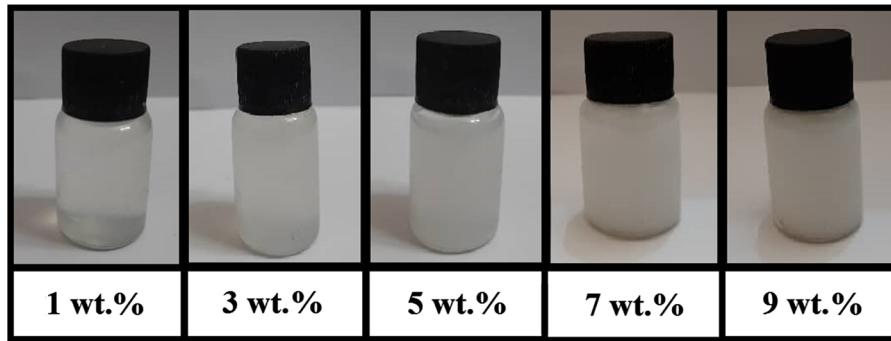To analysis the purity structure of CNF, XRD equipment (Philips Company United Kingdom) was

Fig. 1 Different concentrations of CNF suspension

employed. The XRD data were collected using CuKα radiation. To carry out the test, a dilute suspension containing CNF, (disintegrated by sonication process), was placed in the oven at 60 °C to evaporate the remaining water. Afterward, the sample was introduced to XRD test, and the measurements were carried out in a 2θ range between 10° and 40°.

FTIR spectroscopy

FTIR spectroscopy (Bruker tensor 27, Germany), with a wavelength range of 4000–500 cm^{-1}, was employed to determine the chemical bonds and functional groups in nanocomposites and also to investigate the grafting reaction between AA monomers and St chains. All samples were dehydrated and grounded into powder and mixed with potassium bromide to prepare tablets for FTIR test.

SEM, FE-SEM, and TEM analysis

The morphological structure of the hydrogels before and after the addition of CNF was analyzed using scanning electron microscopy (SEM) images, taken by an FEI Quanta 200 model, USA. Before analysis, the samples were dipped into deionized water for 24 h to reach the equilibrium swelling. Subsequently, the samples were cryogenically immersed and frozen in liquid nitrogen and dehydrated using a freeze-dryer (FD-5003-BT) at − 55 °C for 48 h. Morphological structure of the CNF was also analyzed using FE-SEM images, taken by MIRA3TESCAN-XMU model, Czech Republic. High Resolution-TEM (HR-TEM) images of hydrogels were captured by JSM-7610F JEOL 200 kV, USA. TEM images were also taken by PHILIPS EM208S 100 kV, Netherland, for evaluating

the morphology of hydrogels. To do so, a small droplet of the hydrogel suspension was placed on a grid, and the excess solvent was evaporated at 25 °C.

Compression test

A Hounsfield equipment (Model H25KS, Redhill, England) was employed to measure the compression strength of hydrogels. For this purpose, all samples were swollen by being dipped into water for one night. Then, after removing the extra water, samples were cut into 10 × 10 × 10 mm^3 dimensions and compressed under 500 N at a rate of 1 mm/min and the temperature and relative humidity of 25 °C and 50%, respectively. Equation 2 was used to compute Young's Modulus:

$$Young's\,Modulus = \frac{F \times L_2}{A \times (L_2 - L_1)} \qquad (2)$$

Here F represents the required load (N) for compressing the sample, A shows the area (m^2) of the sample under compression, L_1 and L_2 stand for the initial length of each piece (mm and the length of the sample before failure (mm), respectively (Lee and Chen 2004, 2005; Pahlevan et al. 2018; Xhanari et al. 2011).

Density of hydrogels

Densities of hydrogels were determined using a densitometer instrument (KERN, PLS 360-3, Germany), based on Archimedes' principle. The experiments were performed in triplicates, and the resultant mean values were computed via the Eq. 3. The density of ethanol was assumed to be 0.784 g cm^{-3} in ambient temperature.

$$d_1 = \frac{A}{A - B} d_0 \qquad (3)$$

Here d_1 and d_o represent hydrogel and ethanol densities (g cm^{-3}), A is the hydrogel weight in fluid air (g), and B is the hydrogel weight inside ethanol (g) (Flory and Rehner Jr 1943).

Swelling properties of hydrogels

Equilibrium swelling was investigated through the teabag method. Hence, 0.03 g of each sample was weighed and put into teabags at 25 °C and dipped into distilled water at pH = 8. Subsequently, the swollen hydrogel in the teabag was weighted at 5 min intervals until the system reached a stable amount; before the measurement, extra water was also removed from the teabag. Equation 1 was used for measuring the swelling capacity of samples. Moreover, the swelling capacities of the hydrogels in different saline solutions (0.2 M of NaCl, CaCl$_2$, and AlCl$_3$) were measured in 30 min intervals at 25 °C (Parvathy and Jyothi 2012b). Besides, the influence of pH on the swelling behavior was investigated using the universal buffer solution (boric acid, phosphoric acid, acetic acid, and sodium hydroxide), which provided a pH range of 2 to 12 by varying the NaOH concentration. All hydrogels were put in a buffer solution at 25 °C for 8–9 h. The swelling amount was measured every 30 min.

Biocompatibility test

To sterilize the hydrogel samples, (5 wt% CNF in St-g-PAA hydrogel), three different following steps were passed during the experimentation. The samples were soaked into the ethanol (70 wt%) for 30 min. They were then rinsed with phosphate buffer solution three times with an interval of 5 min (Huang et al. 2018; Kharaziha et al. 2013). Finally, they were irradiated with ultraviolet light for approximately 2 h. The hydrogel samples, after sterilization, were transferred into a flask with an area of 75 cm^2 with 10 mL of culture solution consisting 10% L929 (mouse fibroblasts, 10,000 cells per samples surface for incubation of 1, 3, and 5 days) and 1% Penicillin/Streptomycin and Dulbecco's Modified Eagle's Medium, (DMEM-low) (Huang et al. 2018; Kharaziha et al. 2013). The culture environment was changed every 2 days to facilitate the replication of cells and production of cell

layers over the surface of the flask. After each day, 100 μl of calcein-AM (2 μM) and propidium iodide (4 μM) was added to the hydrogel samples. The final cells were studied by fluorescence microscopy to determine dead/live cells.

Results and discussion

X-ray diffraction analysis

Figure 2 shows the results of XRD test for the used CNF, which used for the preparation of hydrogel. According to the XRD pattern of original CNF, two separate peaks can be observed at $2\theta = 16$ and $22.5°$ indicating the structure of CNF compared to the results presented by French and Cintrón (2013). The XRD patterns of synthesized CNF are in accordance with the literature results and indicating high purity of cellulose within the nano-sized structure (French and Cintrón 2013; Ling et al. 2019).

FTIR spectroscopy

Figure 3 shows the FTIR spectrum of both CNF and hydrogels. The peaks at 3344, 2900, and 1646 cm^{-1} in the CNF spectrum (Fig. 3a) are individually represent the stretching vibrations of hydroxyl groups (–OH), C–H bonds, and –OH in their structure as well as water molecules absorbed by CNF. Also, H–C–H or O–C–H bending in this spectrum appeared at 1432 cm^{-1} (Spagnol et al. 2012c). The peaks at around 1100–1300 cm^{-1} are the distinctive peaks of cellulose; the peak at 898 cm^{-1} can be assigned to the
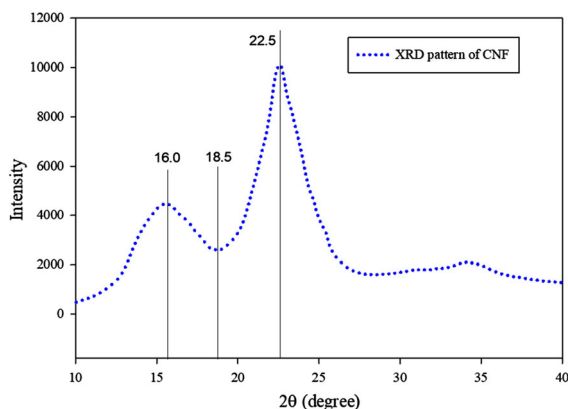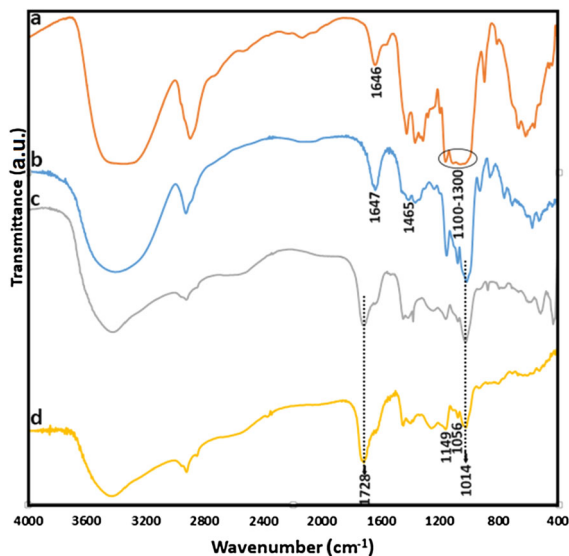
Fig. 2 The results of XRD analysis for CNF

Fig. 3 FTIR spectra of (*a*) CNF, (*b*) St, (*c*) St-*g*-PAA hydrogels, and (*d*) St-*g*-PAA/CNF (5 wt%) hydrogel

functional groups of β-glucosidic linkages between the sugar units. Similarly, a broad peak was found at around 3365 cm^{-1} in the spectrum of St (Fig. 3b) due to the presence of –OH groups of St. The peaks at 1014 and 2930 cm^{-1} can also be ascribed to the stretching vibrations of C–O and C–H bonds, respectively, within the structure of St. The spectrum of the St-*g*-PAA hydrogel (Fig. 3c) also showed the presence of a broad hydroxyl peak in the range of 3500 to 3300 cm^{-1}. Furthermore, there existed a strong peak at 1728 cm^{-1} because of the stretching vibration of the ester bonds (C=O) existing in carboxyl groups. Furthermore, the peaks at around 1723 and 1406 cm^{-1} can be attributed to the stretching vibration of C=O. These peaks are mainly appeared due to the –COOH groups and symmetrical and asymmetrical stretching vibrations of carboxylate groups (COO$^-$). These observations illustrated that the polymerization of AA monomers grafted onto the backbone of St had some positive effects on the COOH and COO$^-$ groups of hydrogels, which consequently resulted in the better swelling behavior of hydrogels. The peak at 1585 cm^{-1} was revealed the CO stretching vibrations of COONa groups. This peak appeared after the alkaline hydrolysis (neutralization) of some –COOH groups using NaOH solution (Li et al. 2005). The peaks at 1647 and 1465 cm^{-1} were disappeared after graft polymerization, similar to the results obtained by

Güler et al. (2015) who studied St-*g*-PMMA hydrogels. Moreover, adding CNF into the hydrogels (Fig. 3d) showed the distinctive peaks of cellulose as well as some extra peaks at 1149 and 1056 cm^{-1}, which were the result of the asymmetrical vibrations of C–O–C and stretching vibrations of C–C and C–O asymmetric pyrin ring. The peak at 1646 cm^{-1} disappeared after the interaction of St and CNF. These results were in agreement with those achieved by Spagnol et al. (2012c) who investigated the influence of CNF on chitosan-based hydrogels.

Hydrogel and CNF morphology

The morphologies of the unreinforced and 5 wt% CNF-reinforced hydrogels were studied using SEM micrographs. As depicted in Fig. 4a, the surface of the unreinforced St-*g*-PAA hydrogels formed small homogenous voids with a diameter varying between 23 and 215 μm, calculated by Image J software version 2016. Figure 4b portrays the irregular appearance of the reinforced St-*g*-PAA hydrogel with more appreciable inhomogeneous voids and more interconnected networks with a diameter ranged between 20 and 112 μm. Decreasing the diameter of voids increases the diffusion of the solution into hydrogels mainly because of enhancing the pressure and diffusion forces. Figure 4c depicts a micro section of the St-*g*-PAA/CNF hydrogel with probably a bundle of CNF with 81 nm diameter attached on the surface of St-*g*-PAA, implying the good interactions between the CNF and the matrix. Based on the images, it can be noticed that CNF loading pronouncedly influenced the morphology of hydrogels and increased the number of voids that led to a highly porous structure, appealing for improving the water absorption capacity of hydrogels (Bian et al. 2018; Sethi et al. 2017; Spagnol et al. 2012b; Wang et al. 2015; Xia et al. 2013; Zhao et al. 2013). It can also be said that the presence of CNF within matrix increased the number of hydrophilic groups, allowing biological solutions to penetrate into the hydrogel network more easily. In a similar research, the influence of CNF on the morphology of hydrogels was investigated (Spagnol et al. 2012c).

Figure 5a, b respectively depict the TEM and HR-TEM of the as-prepared nanocomposite. As can be observed, the existence of voids in the hydrogel (Fig. 5a1, b) and also the presence of CNF (Fig. 5a2)
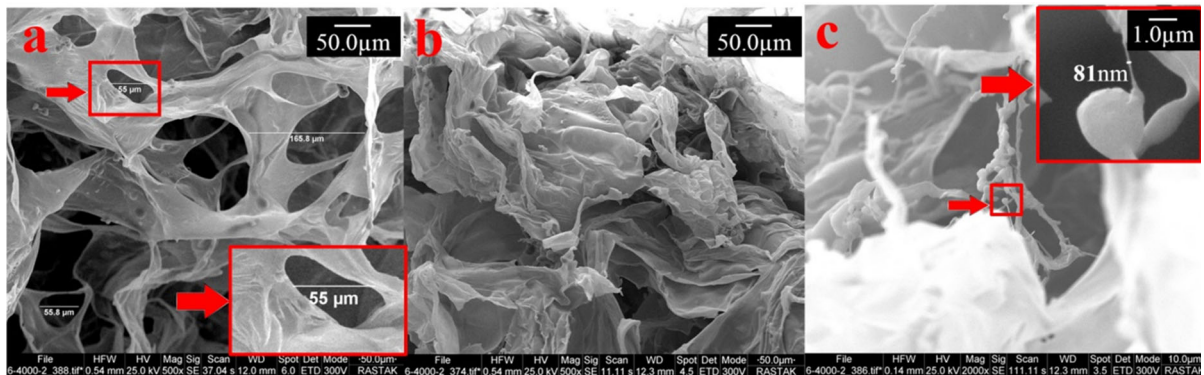
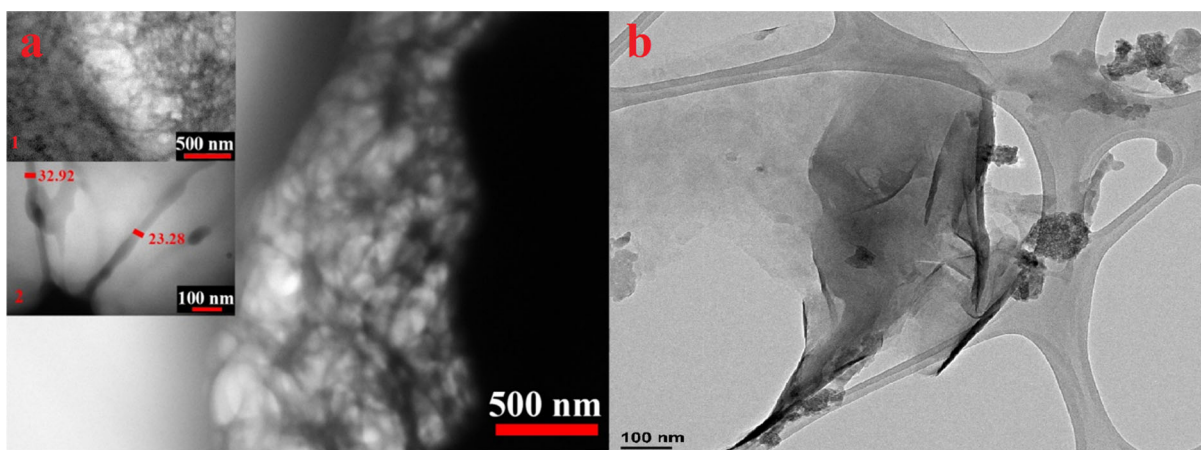**Fig. 4** SEM images of **a** St-*g*-PAA and **b** and **c** St-*g*-PAA/CNF hydrogel

Fig. 5 **a** TEM and **b** HR-TEM images of St-*g*-PAA/CNF hydrogel

are easily distinguishable (Bian et al. 2018). According to the results, it can be concluded that the average diameter of CNF is less than 50 nm indicating the proper distribution of CNF during the production of reinforced hydrogel.

Figure 6a and b also show the morphological structure, (obtained from FE-SEM analysis), as well as mean diameter distribution of CNF with an average diameter within the range of 18–48 nm, calculated by OriginLab software version 2018 (more information is available in the Supplementary Information: Section C and Scheme. S1).

Optimization of St-*g*-PAA graft polymerization

Here, Design-Expert® software (version 7.0.0) was employed to optimize the polymerization parameters. Based on the ANOVA results, the F-value (8.66) and P

value (0.0066) of the proposed model are reliable; as an example, *P*-value less than 0.05 is the indication of the model reliability. Adequate precision (8.356), the R-square (0.8608), adjusted R-square (0.7614), and modified R-square (0.6464) are other significant indices to prove the reliability of the models (Table S2). The most effective parameters of the model in respect to the F-value and *P*-value are A^2, A, B, B^2, and AB (Table S2). It is worth noting that 0.80 is the lowest R-square value for a good fit of a model (Baboukani et al. 2012). Furthermore, the model precision is adequate when the provided ratio of the predicted values is greater than 4.0 at the design points to the average prediction error. The rest of the statistical parameters also confirmed the accuracy of the proposed model. The model proposed by the software is a quadratic response surface model, where it is approximately fit with the experimental data
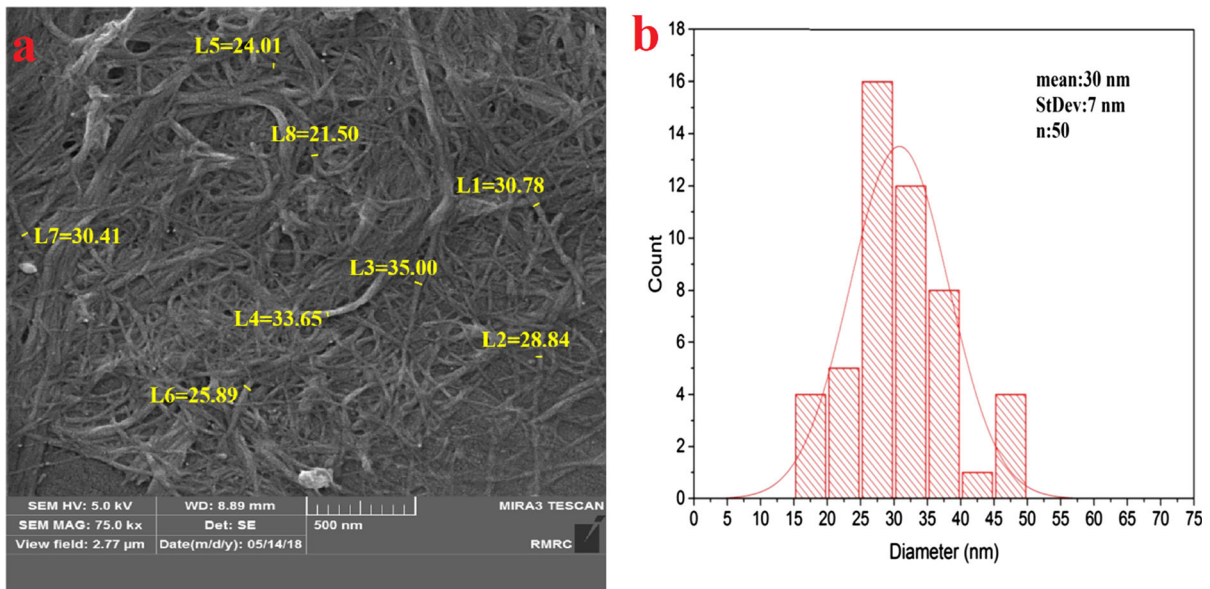
Fig. 6 **a** FE-SEM image of CNF and **b** average diameter distribution of CNF

(Fig. S1a-b). The relation between the main effective parameters and interactions of ratios of AA/St and MBA are shown in the following equation in a coded form:

$$Swelling = -362.08 + 35.05 \times A + 15.76 \times B \\ + 4.17 \times A \times B - 49.17 \times A^2 - 13.87 \\ \times B^2$$

(4)

Optimum values, for the monomer and cross-linker, were respectively found to be 3.65 g AA per 1 g St and 1.12 wt% MBA. Under these conditions, the swelling was predicted to be 292.47 g/g, equivalent to just 7% errors compared to the experimental value (312 g/g), thus, the accuracy of the model appears to possess a high degree of reliability (more information is available in the supplementary: Section A, B, and C).

Biocompatibility of composite

To estimate the biocompatibility of the nanocomposite hydrogels, Mouse L929 fibroblastic cells were cultured on the surface of both reinforced and unreinforced hydrogels according to the literature (Boateng et al. 2003; Huang et al. 2018; Kharaziha et al. 2013). Figure 7a exhibits that the hydrogel has some cluster structures. The fluorescent image of live mentioned cells with green color and dead ones with

red color is shown in Fig. 7b. It can be observed from this image that cells grew well on the reinforced hydrogel and exhibited a high population after passing 5 days (Huang et al. 2018; Kharaziha et al. 2013). Moreover, a small number of red cells were observed, lower than 5% of the overall population.

Figure 8 shows a comparison between the reinforced and unreinforced hydrogel and the fraction of live and dead cell on their surface after passing 1, 3, and 5 days. The results presented in this figure exhibit that with increasing the time from 1 day to 5 days, the numbers of live cells were increased in both reinforced and unreinforced hydrogel declaring the high degree of biocompatibility of hydrogels. However, these results showed that the fraction of live cells on the surfaces of the reinforced hydrogel is higher than unreinforced one. This results showed that CNF significantly enhanced the biocompatibility property of hydrogel, and thus, it can be used for cell proliferation. Cellulose nanofibers extremely are categorized as biocompatible materials that can be used in medical application. From this part of research, it can also be noticed that by adding CNF into hydrogel the biocompatibility of hydrogel nanocomposite is increased compared to the blank sample (without CNF). Dugan et al. (2010) clearly showed that myoblasts could sense the topography of surfaces of tunicin CNWs effectively and orientate relative to the
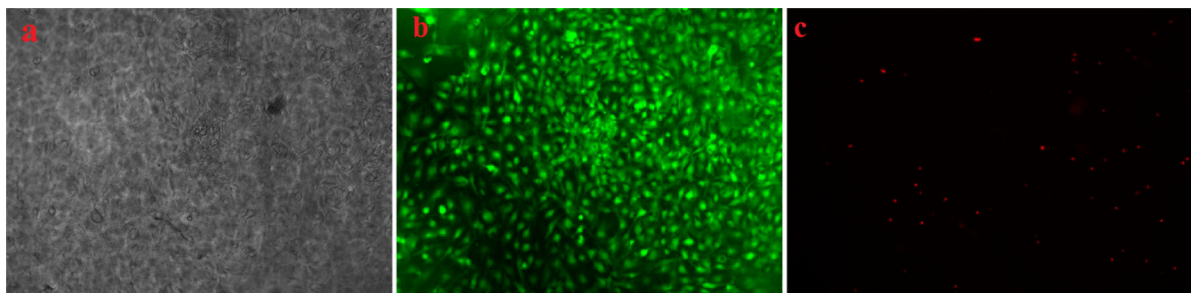
Fig. 7 **a** Fluorescence microscopy images of the reinforced hydrogel and **b** live cells cultured on the reinforced hydrogel after 5 days **c** dead cells after 5 days
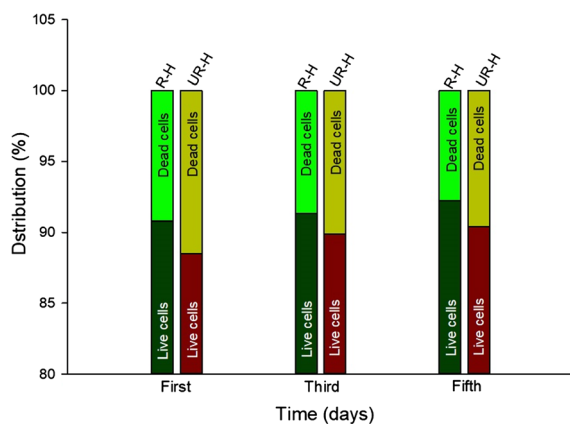

Fig. 8 The comparison between the proliferation of live cells on the surface of reinforced (R-H) and unreinforced hydrogels (UR-H)

Fig. 9 Influence of CNF on the compression strength and Young's modulus of St-*g*-PAA/CNF hydrogel with different amount of CNF

bulk direction of CNWs orientation. Their results absolutely show that cellulose molecular structures can increase proliferation of live cell leading to enhance the biocompatibility of hydrogel matrix.

Mechanical properties of composite

The mechanical properties of CNF-based hydrogels are presented in Fig. 9. As can be concluded, the incorporation of 1 wt% CNF in the matrix decreased both compression strength and Young's modulus of hydrogels, because CNF cause more water absorption ability than enhancing mechanical strength to the hydrogel at low concentrations. While this trend disappeared at 3 and 5 wt% of CNF. The latter decrease in the mechanical properties can be referred to the enhanced water absorption at this concentration. Based on the results, the compression strength and modulus of hydrogel with 5 wt% of CNF were increased by about 69% and 140%, respectively,
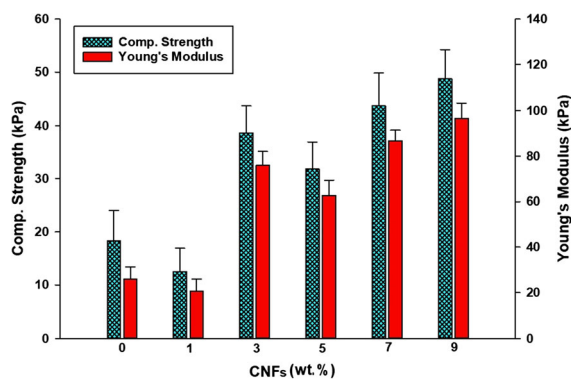
compared to the unreinforced hydrogel. Also, at higher concentration of CNF (more than 5 wt%), mechanical properties were increased once again. Formation of a rigid network by overloading CNF can account for such an observation. The enhancement in hydrogel nanocomposites performance can be attributed to the higher and stronger mechanical properties of applied CNF and the high degree of intramolecular interaction between CNF' surface and St-*g*-PAA hydrogel network, leading to a higher amounts of stress transfer from the hydrogel polymer network to the CNF which are acting as nanofillers (Huang et al. 2018). The ultimate reinforcing content of CNF was observed at 9 wt%, in which the compression strength and Young's modulus were found to be 48.15 ± 5 and 96.3 ± 6 kPa, respectively. Spagnol et al. (2012b) also found similar results with the incorporation of CNW in hydrogels as Young's modulus was reached to 40 kPa at 20 wt% of CNW.

Swelling properties of hydrogels

The relationship between the addition of CNF with different weight percentages (1, 3, 5, 7, 9 wt%) in hydrogel and the swelling behavior of the resultant samples, which were synthesized under the optimal conditions, is depicted in Fig. 10. As can be observed, the incorporation of CNF up to 5 wt% into the hydrogels increased their equilibrium swelling at 25 °C up to 523 ± 14 g/g, which is 67% higher than the equilibrium swelling of St-*g*-PAA hydrogel (312 ± 11 g/g).

This improvement can be attributed to the presence of OH groups in the backbone of cellobiose, the smallest repetitive unit of CNF, which could potentially address the hydrophilic character of the reinforced hydrogels. Furthermore, proper distribution of CNF within polymeric matrix could inhibit the entanglement of polymeric chains and decrease the interactions among the hydrophilic groups of the matrix, including –OH, –COOH, and –COO⁻. This phenomenon decreased the degree of physical cross-linking in the network and increased the favorable sites appealing for the absorption and retention of water molecules (de Azevedo et al. 2017; Sethi et al. 2017; Spagnol et al. 2012b, c). As results displayed, over-inclusion of CNF (> 5 wt%) reduced the swelling capacities of hydrogels by 25–30%. Even though there exist some likely explanations behind this, the most probable reason would be the interference of some of –OH groups of CNF in the graft polymerization of PAA (Spagnol et al. 2012a, b). This led to increase the number of unwanted cross-linking

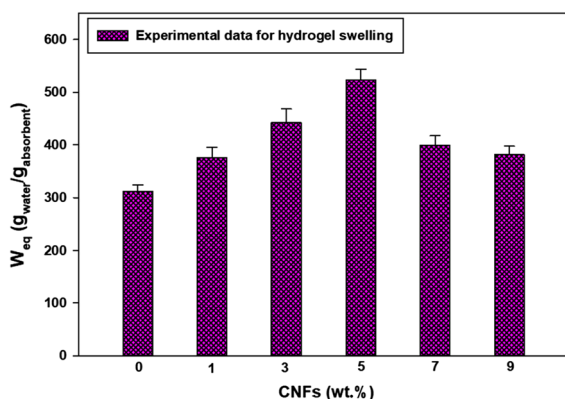reactions in the polymeric network and decrease available volumes as well as hydrophilic groups, (of matrix per volume unit), which were able to partake freely in the retention of water molecules. Another possible reason could be the increase in agglomerations that declined the swelling capacity of the hydrogels. These observations were in agreement with the results obtained by Spagnol et al. (2012a). Also, the density of the hydrogel nanocomposites reinforced by 5 wt% of CNF was found to be 1.01 g cm⁻³. The dimensionless swollen volume of the 5 wt% CNF-reinforced hydrogels calculated by Eq. 5, was found to be 529.28.

$$SV = \frac{\frac{W_2 - W_1}{d_s}}{W_1 / d_p} \tag{5}$$

Here SV shows the swelling volume, d_s stands for the water density, d_p represents the hydrogel density, w_1 (g) is the weight of the dried hydrogel, and w_2 (g) shows the weight of swollen hydrogels. The polymer volume fraction (v_p) of swollen hydrogels in an equilibrium condition was calculated by the inverse value of the dimensionless swollen volume (529.28). In the present study, this value was lower than that of the sample reinforced by microcrystalline cellulose (MCC) (Table S3) (Xhanari et al. 2011). The water volume fraction (v_s), which is ($1 - v_p$) for the CNF-reinforced hydrogels, was higher than that of the MCC reinforced sample, revealing the higher ability of CNF which cause higher absorption of hydrogels (Flory and Rehner Jr 1943; Xia et al. 2013).

Effect of salt solutions

The retention ability of hydrogels reinforced by 5 wt% CNF was examined in different salt solutions (0.2 M). As Fig. 11 shows, swelling of CNF-reinforced St-*g*-PAA hydrogels in NaCl, CaCl₂, and AlCl₃ solutions were found to be 193 ± 9, 110 ± 8, and 99 ± 7 ($g_{water}/g_{absorbent}$), respectively. Similarly, these values for the unreinforced St-*g*-PAA hydrogels were obtained to be 109 ± 8, 62 ± 7, and 56 ± 6 ($g_{water}/g_{absorbent}$), respectively. Results showed that different ions impacted the swelling behavior of superabsorbent hydrogels, and the absorption of hydrogels exposed to various aqueous salt solutions was completely contingent upon the ionic strength of monovalent, divalent or trivalent salt. Furthermore, the swelling of the
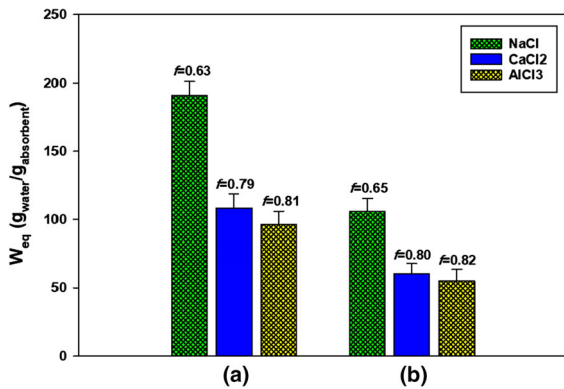

Fig. 10 The influence of the loading of CNF on the ultimate swelling of the St-*g*-PAA hydrogels

Fig. 11 Water absorption ability of the hydrogels in different salt solutions (NaCl, CaCl₂, and AlCl₃): **a** St-*g*-PAA/CNF (5 wt%) hydrogel and **b** unreinforced St-*g*-PAA hydrogel at pH = 8

hydrogels in the salt solutions was lower than that of their counterparts in water, and the incorporation of CNF resulted in 77% improvement in the absorption capacity of the hydrogels compared to the unreinforced one. It is also worth noting that the highest absorption took place when hydrogels were immersed in monovalent salt, and the lowest absorption was found in trivalent one. Thus, it can be concluded that higher ionic strength of salt solution interacted more with the hydrogel, which led to a significant reduction in the osmotic pressure between solution and hydrogel matrix. This potentially would increase the ionic interactions and leads to more contraction due to the internal ionic attraction force. Therefore, this decreases free volumes, and consequently, decreases the swelling capacity of hydrogels (Li et al. 2005; Parvathy and Jyothi 2012b).

As shown in Fig. 11 dimensionless salt sensitivity factor (f = 1 − (swelling capacity of the hydrogel in a salt (S_s)/swelling capacity in pure water (S_w))) can provide a comprehensive picture regarding to how different cations from different salt solutions with the same concentration can influence the ion-exchange ability of the hydrogels. Accordingly, for f equal to 1, the maximum ionic sensitivity of salt solutions, or minimum swelling capacity of hydrogels is observed (Parvathy and Jyothi 2012b). As can be concluded, the influence of ionic solutions on the water absorption of CNF-reinforced hydrogels was lower than that of the unreinforced ones. The f values for the St-*g*-PAA/CNF (5 wt%) hydrogels in NaCl, CaCl₂, AlCl₃ solutions were found to be 0.63, 0.79, and 0.81, respectively,

and for the unreinforced counterparts were also calculated to be 0.65, 0.80, and 0.82, respectively. The significant differences between S_s and S_w can be probably ascribed to the differences of the osmotic pressures of the hydrogels and the external salt solutions.

Regarding the swelling behavior of hydrogels, it can also be pointed out that the tendency toward water absorption declined with the augmentation of ionic strength in salt solutions. This declination was more tangible in multivalent cationic solutions (Ca²⁺ and Al³⁺) as they seemingly possessed the ability to form intra and intermolecular complexes with carboxylate groups, leads substantially to cross-link density enhancement of the network and consequently contraction of hydrogel (Li et al. 2005). Furthermore, as these cationic ions could cover some carboxylate groups, available in the hydrogels, the anion–anion repulsive forces would decline which decrease the water absorption (Parvathy and Jyothi 2012b). However, the presence of CNF enhances the anion–anion repulsive forces, thereby improving the swelling capacity of the hydrogels (Spagnol et al. 2012a, c).

Effect of pH on the water absorption

Figure 12 represents the water absorption growing in both reinforced and unreinforced hydrogels with increasing pH from 2 to 8; however, swelling capacity was decreased by increasing pH above 8. As can be observed, water absorption appeared to be low in acidic conditions, (pH < 4). One probable explanation regarding to this observation is probably due to
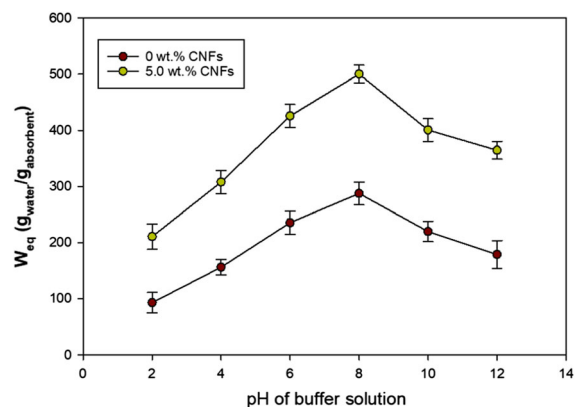

Fig. 12 Equilibrium swelling capacity of St-*g*-PAA/CNF (5 wt%) and unreinforced St-*g*-PAA hydrogels at various pH

the conversion of carboxylate groups (–COO⁻) to the carboxylic acid groups (–COOH), provoking hydrogen bond-based interactions between –COOH and –OH groups, augmenting the cross-linking density of the network. This can also be verified using the model presented by Flory–Huggins (more information is available in the Supplementary Information: Section B) (Chen and Tan 2006; Li et al. 2008). It can be concluded from this model that as the cross-linking density increases, the swelling capacity decreases. Besides, with the rise in pH from 4 to 8, lower hydronium ions can be produced in solution leading to a significant conversion of some –COOH to –COO⁻ causing more anion–anion repulsive forces of polymer chains, enhancing the expansion of the matrix and the swelling capacity of the hydrogels as well. The highest value of water absorption was occurred at pH 8 for nanocomposite (5 wt% CNF) hydrogel (502 ± 14 g/g) and unreinforced hydrogel (291 ± 11 g/g). These values corresponded to 72% increment in water retention ability of CNF-based hydrogels. On the other hands, by increasing pH from 8 to 12, the water absorption was decreased. This reduction can be primarily ascribed to higher osmotic pressure phenomenon, competing anions in solution and hydrogel, and the ionization of hydrogel networks in pH ranging from 10 to 12. This is due to the induced destructive screening influence, declining the electrostatic repulsive forces inside the hydrogel and collapsing the polymer networks (more information is available in the Supplementary Information: Section D and Fig. S2) (Bardajee and Hooshyar 2013; Bidgoli et al. 2010).

Water absorption kinetics

As observed in Fig. 13, although the amount of absorption followed similar trends in both samples, CNF had a considerable influence on the swelling kinetics of hydrogels. During the first 30 min, about 63% of the maximum absorption for the CNF-reinforced hydrogel and about 47% for the unreinforced counterpart were achieved at the equilibrium point; after that, the swelling capacity was almost remained constant. Accordingly, the incorporation of CNF into the St-*g*-PAA hydrogel network increased water absorption capacity of hydrogels and reduced the equilibrium time in such a way that the amount of the time needed for reaching 90% of maximum
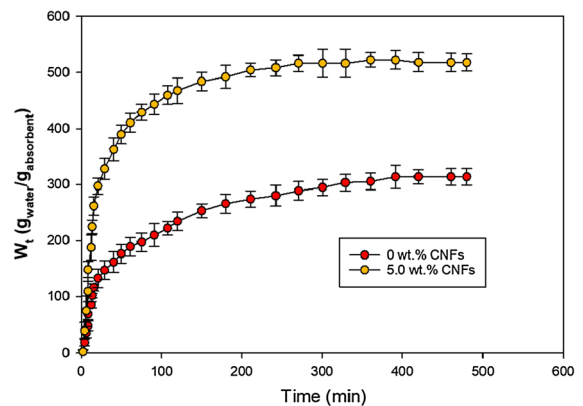

Fig. 13 Water absorption kinetics data for the reinforced and unreinforced St-*g*-PAA hydrogels at pH = 8

absorption in CNF-reinforced hydrogels was approximately 120 min, while this period for the unreinforced counterparts was found to be 240 min.

Swelling at the equilibrium point for the 5 wt% CNF-reinforced and unreinforced hydrogels were found respectively to be 523 ± 14 and 312 ± 11 $g_{water}/g_{absorbent}$. To verify the influence of CNF on the swelling kinetics of hydrogels, Schott's pseudo-first-order, (Eq. 6), and pseudo-second-order models, (Eq. 7), were studied (de Azevedo et al. 2017; Ho and McKay 1998; Schott 1992).

$$log\left(W_{eq} - W_t\right) = logW_{eq} - k_1t/2.303 \qquad (6)$$

$$t/W_t = 1/k_2W_{eq}^2 + t/W_{eq} \qquad (7)$$

Here W_t and W_{eq} (g/g) stand for the amount of absorption at time t and in equilibrium, respectively. k_1 (min⁻¹) and k_2 (g g⁻¹ min⁻¹) are Schott's pseudo-first and second-order rate constants, respectively. The experimental swelling trend of data, based upon the pseudo-first and second-order models, are exhibited in Figs. 14 and 15. By fitting data with models and mapping, kinetics parameters related to each model and correlation coefficients (R^2) were calculated (Tables 2 and 3). According to the data obtained from Fig. 14 and Table 2, the pseudo-first-order kinetics model could not sufficiently describe the kinetics behavior of samples. As can be explicitly seen, the experimental data in the first and middle steps were approximately fit with the model, however, by passing the time especially over 120 min for the unreinforced sample and 180 min for the reinforced counterpart, the accuracy of this model for prediction was decreased.
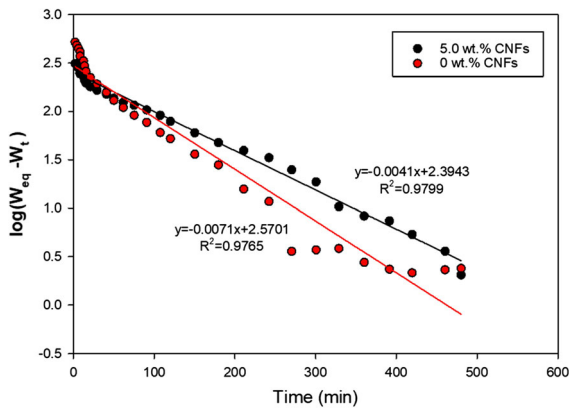
Fig. 14 Pseudo-first-order kinetics model for the reinforced and unreinforced St-*g*-PAA hydrogels at pH 8
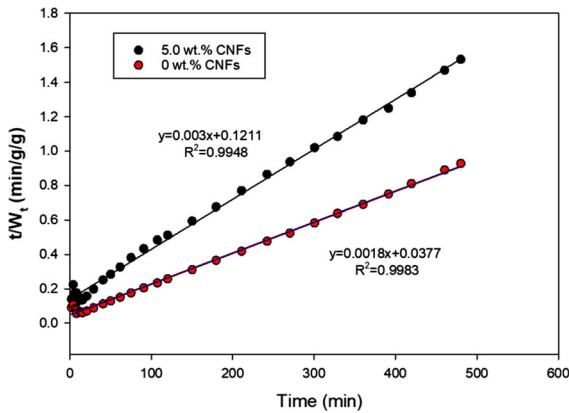

Fig. 15 Pseudo-second-order kinetics model for reinforced and unreinforced St-*g*-PAA hydrogels at pH 8

The rate constants, based on this model, for the reinforced and unreinforced hydrogels, were calculated to be 9.44×10^{-3} and 1.6×10^{-2} min^{-1},

respectively. According to the results obtained from data presented in Table 2, it can be noticed that the value of maximum absorption obtained from calculation differs significantly from experimental value for both reinforced and unreinforced hydrogel declaring lower precision of this model for prediction of experimental data.

The observed lack of fit between the experimental data and the pseudo-first-order kinetics model, based on Eqs. 8 and 9, (Schott 1992) can be justified by the rate constant k_1 or k having a direct relationship with the diffusion coefficient, D (dimension), and an inverse relation with the hydrogel thickness H (dimension).

$$ln\left(\frac{W_{eq}}{W_{eq} - W}\right) \cong \frac{\pi^2 D \cdot t}{H^2} \tag{8}$$

$$\frac{k_1}{2.303} = k = \frac{\pi^2 D}{H^2} \tag{9}$$

D and H^2 values were gradually increased during the absorption process and k value was remained constant. A sudden increase in D value at a time approximately equal to 240 min (for the unreinforced sample) and 330 min (for the reinforced one) can be explained by the reduction of glass transition temperature (T_g) of hydrogels below the experimental temperature, caused by water molecules. This can explain the appropriate response to the swelling behavior of hydrogels only in the first and middle of the experiment. The presence of CNF in the hydrogel had a positive influence on the increment of k and D compared to the unreinforced one.

Furthermore, when absorption reached its climax, the increase in the size of hydrogel exceeded the

Table 2 Kinetics parameters of absorption for the pseudo-first-order kinetics model

CNF (%)	$W_{eq(exp)}$ (g/g)	$W_{eq(Cal)}$ (g/g)	k_1 (min^{-1})	R^2
0	312	247.91	9.44×10^{-3}	0.9799
5	523	371.62	1.6×10^{-2}	0.9765

Table 3 Kinetics parameters of absorption for the pseudo-second-order kinetics model

CNF (%)	$W_{eq(exp)}$ (g/g)	$W_{eq(Cal)}$ (g/g)	k_2 (min^{-1})	k_{is} (g/g/min)	R^2	$t\frac{1}{2}$ (min)
0	312	333.33	7.43×10^{-5}	8.2553	0.9948	43.13
5	523	555.55	8.59×10^{-5}	26.5118	0.9983	22.25

diffusion coefficient D due to water penetration (H parameter). This resulted in a significant deviation from the pseudo-first-order kinetics model (Schott 1992). Therefore, the absorption kinetics study on each hydrogel using the pseudo-second-order kinetics model revealed an acceptable match with the experimental data (R^2 = 0.99) (Fig. 15). Table 3 summarizes the parameters extracted from the pseudo-second-order kinetics model. As can be observed, the graphs were linear in this model, justifying the swelling behavior of samples during the swelling period, even at high swelling amounts. This model is in a good agreement with experimental results which confirm strong interactions between the absorbent and absorbate. The number of theoretical equilibrium swelling values, calculated from the graphs for the reinforced and unreinforced hydrogels, were found to be 333.33 and 555.55 (g/g), close to the experimental equilibrium swelling values. The low deviation of the theoretical values from the experimental ones and the proper ability of the pseudo-second-order model in describing the swelling behavior of samples is observed.

The swelling rate constant of hydrogels containing CNF was found to be 8.59×10^{-5} min^{-1} which compared to the unreinforced hydrogels (7.43×10^{-5} min^{-1}) revealed the higher swelling rate to reach to the equilibrium. The initial rate of swelling (k_{is}) was calculated according to Eq. 10 (Ho and McKay 1998).

$$k_{is} = k_2 W_{eq(Cal)}^2 \qquad (10)$$

These values for the unreinforced and reinforced hydrogels were found to be 8.25 and 26.51 (g/g min). The half-life ($t_{1/2}$) indicates the time when samples absorb half of the water amount (as a solvent). Based on Eq. 11 (de Azevedo et al. 2017), the value of this parameter for the unreinforced and reinforced hydrogels were found to be 22.25 and 43.13 min, respectively. Therefore, the initial velocity and half-life of the samples confirmed the higher swelling rate of hydrogels containing CNF. These results were similar to those obtained by Spagnol and Dai (Dai and Kadla 2009; Spagnol et al. 2012c).

$$t_{1/2} = \frac{1}{k_2 W_{eq(exp)}} \qquad (11)$$

Furthermore, the swelling behavior of hydrogels can be studied based on transition mechanisms.

Generally, absorption of water molecules by a hydrogel happens in two ways: first, Fick's law of diffusion, which concerns the diffusion and random movement of solvent molecules into hydrogel's polymeric network. The absorption capacity depends on some parameters such as temperature, pressure, concentration gradient, pH, etc. Second, the relaxation mechanism of a hydrogel's polymer chain (non-Fick diffusion), which allows absorption of water molecules into a hydrogel. In other words, the mobility of hydrogel molecules picks up to the extent that allows absorption through physiochemical interactions inside the hydrogel. Values for diffusion power (n)—the indicator of diffusion type—and D are shown in Fig. S3 and are computed by Korsmeyer–Peppas equation (Reis et al. 2008), ($F = W_t/W_{eq} = Dt^n$), for two samples of the unreinforced and the 5 wt% CNF-reinforced hydrogels. This model showed that the behavior of the samples is almost linear up to 40–50% of the swelling process (Fig. S3). After this point, the process is non-linear, and the model is not adequate in describing the behavior of the samples, especially for CNF-reinforced hydrogel. Nevertheless, values of n were calculated by drawing the best line crossing the curves of the samples. Also, n values in both samples follow Fick's law of diffusion since n < 0.45 indicates Fick's diffusion while n values 0.45 < n < 0.89 indicate both Fick's diffusion and relaxation mechanism. In addition, high values of D confirmed high absorption of CNF-reinforced hydrogel, (Table S4) (Nawang et al. 2001; Reis et al. 2008).

Comparison with previous researches

According to the data presented in Table 4, it can be concluded that the nanocomposite hydrogel investigated in this study shows a high degree of water absorption, mechanical properties, and biocompatibility. Although the maximum water absorption was achieved from St-g-PAAm/attapulgite, however, the compatibility test was not carried out on this sample. Besides, another research confirmed the biocompatibility of CNF/P(AAm-co-AAc) hydrogel, (showing 90% culture of living cells), and high mechanical properties. Therefore, it can be concluded that CNF/St-g-PAA hydrogel have good mechanical and swelling properties alongside with high biocompatibility (93% of living cells).

Table 4 Comparison between other previous research and the present study

Authors	Maximum swelling ($g_{water}/g_{absorbent}$)	Biocompatibility	Mechanical properties	Hydrogel	Refs.
Güler et al.	21.9	Not reported	C/E^a = 0.168	10Mt/St-g-PMAA	Güler et al. (2015)
Bardajee et al.	650	Not reported	Not reported	MION-PAA-g-St	Bardajee and Hooshyar (2013)
Hamidian et al.	630	Not reported	Not reported	Fe_3O_4/St-g-Polyester	Hamidian and Tavakoli (2016)
Huang et al.	Not reported	Alive cells: 90%	TM^b = 3.4	CNF/P(AAm-co-AAc)	Huang et al. (2018)
Li et al.	1320	Not reported	Not reported	St-g-PAAm/attapulgite	Li et al. (2005)
Parvathy et al.	320	Not reported	Not reported	Cassava St-g-PAAm	Parvathy and Jyothi (2012a)
This study	530	Alive cells: 93%	CS^c = 32	CNF/St-g-PAA	

[a]C/E: Maximum compressive strength (N) per maximum elongation (%)

[b]TM: Tensile modulus (MPa)

[c]CS: Compressive strength (kPa)

Conclusions

In this research, St-g-PAA hydrogels were first successfully synthesized by the optimal amounts of monomers and cross-linker employing designing experimental method (RSM). The synthesized hydrogel was then reinforced by CNF addition. The nanocomposite characterizations revealed that adding CNF up to 5 wt% improved swelling capacity which can be probably explained by the hydrophilic nature of cellobiose units in the structure of cellulose due to the existence of hydroxyl groups. Also, FTIR, SEM, FE-SEM, TEM, and HR-TEM images clearly showed physiochemical and morphological modifications of hydrogels. The results of experimental studies showed that by adding CNF over 1 wt%, the better mechanical properties could be achieved. In addition, CNF-reinforced hydrogels presented well responses to pH variations and salts presence in absorbates. The osmotic pressure and electrostatic repulsion force caused changes in the swelling capacity, a finding that can be of great potentials in controlled release of solutes in biomedical and environmental applications. Furthermore, the kinetics study was in agreement with the pseudo-second-order model. The results of biocompatibility analysis also showed that live cells could proliferate well on the surface of reinforced hydrogel significantly compared to the unreinforced

samples. The results presented in this study exhibited that by increasing the time from 1 to 5 days, the numbers of live cells were increased on both reinforced and unreinforced hydrogel, declaring the high degree of biocompatibility of hydrogels. However, it was also confirmed that the fraction of live cells on the surface of the reinforced hydrogel is higher than the unreinforced sample.

Data availability The data needed to reproduce these results cannot be shared at this time because of the time limitations.

References

Aouada FA, de Moura MR, Orts WJ, Mattoso LH (2011) Preparation and characterization of novel micro-and nanocomposite hydrogels containing cellulosic fibrils. J Agric Food Chem 59:9433–9442

Baboukani BS, Vossoughi M, Alemzadeh I (2012) Optimisation of dilute-acid pretreatment conditions for enhancement sugar recovery and enzymatic hydrolysis of wheat straw. Biosyst Eng 111:166–174

Bakhshi H, Darvishi AJD, Treatment W (2016) Preparation and evaluation of hydrogel composites based on starch-g-PNaMA/eggshell particles as dye biosorbent. Desalin Water Treat 57:18144–18156

Bardajee GR, Hooshyar Z (2013) A novel biocompatible magnetic iron oxide nanoparticles/hydrogel based on poly (acrylic acid) grafted onto starch for controlled drug release. J Polym Res 20:298

Bian H, Jiao L, Wang R, Wang X, Zhu W, Dai H (2018) Lignin nanoparticles as nano-spacers for tuning the viscoelasticity of cellulose nanofibril reinforced polyvinyl alcohol-borax hydrogel. Eur Polym J 107:267–274

Bidgoli H, Zamani A, Taherzadeh MJ (2010) Effect of carboxymethylation conditions on the water-binding capacity of chitosan-based superabsorbents. Carbohydr Res 345:2683–2689

Boateng SY, Hartman TJ, Ahluwalia N, Vidula H, Desai TA, Russell B (2003) Inhibition of fibroblast proliferation in cardiac myocyte cultures by surface microtopography. Am J Physiol-Cell Physiol 285:C171–C182

Chen Y, Tan H (2006) Crosslinked carboxymethylchitosan-g-poly (acrylic acid) copolymer as a novel superabsorbent polymer. Carbohydr Res 341:887–896

Dai Q, Kadla JF (2009) Effect of nanofillers on carboxymethyl cellulose/hydroxyethyl cellulose hydrogels. J Appl Polym Sci 114:1664–1669

de Azevedo AC, Vaz MG, Gomes RF, Pereira AG, Fajardo AR, Rodrigues FH (2017) Starch/rice husk ash based superabsorbent composite: high methylene blue removal efficiency. Iran Polym J 26:93–105

Deng Y, Wang H, Zhang L, Li Y, Wei SJ (2013) In situ synthesis and in vitro biocompatibility of needle-like nano-hydroxyapatite in agar-gelatin co-hydrogel. Mater Lett 104:8–12

Dugan JM, Gough JE, Eichhorn SJ (2010) Directing the morphology and differentiation of skeletal muscle cells using oriented cellulose nanowhiskers. Biomacromolecules 11:2498–2504

Fajardo AR, Fávaro SL, Rubira AF, Muniz ECJR, Polymers F (2013) Dual-network hydrogels based on chemically and physically crosslinked chitosan/chondroitin sulfate. React Funct Polym 73:1662–1671

Ferreira F, Dufresne A, Pinheiro I, Souza D, Gouveia R, Mei L, Lona LJ (2018) How do cellulose nanocrystals affect the overall properties of biodegradable polymer nanocomposites: a comprehensive review. Eur Polym J 108:274–285

Flory PJ, Rehner JJ Jr (1943) Statistical mechanics of cross-linked polymer networks I. Rubberlike elasticity. J Chem Phys 11:512–520

French AD, Cintrón MS (2013) Cellulose polymorphy, crystallite size, and the segal crystallinity index. Cellulose 20:583–588

Gomes RF, de Azevedo ACN, Pereira AG, Muniz EC, Fajardo AR, Rodrigues FH (2015) Fast dye removal from water by starch-based nanocomposites. J Colloid Interface Sci 454:200–209

Güler MA, Gök MK, Figen AK, Özgümüş S (2015) Swelling, mechanical and mucoadhesion properties of Mt/starch-g-PMAA nanocomposite hydrogels. Appl Clay Sci 112:44–52

Hamidian H, Tavakoli T (2016) Preparation of a new Fe3O4/starch-g-polyester nanocomposite hydrogel and a study on swelling and drug delivery properties. Carbohydr Polym 144:140–148

Ho Y, McKay G (1998) A comparison of chemisorption kinetic models applied to pollutant removal on various sorbents. Process Saf Environ Protect 76:332–340

Hoffman AS (2012) Hydrogels for biomedical applications. Adv Drug Deliv Rev 64:18–23

Huang S, Zhao Z, Feng C, Mayes E, Yang J (2018) Nanocellulose reinforced P (AAm-co-AAc) hydrogels with improved mechanical properties and biocompatibility. Compos Part A Appl Sci Manuf 112:395–404

Jahanbaani AR, Behzad T, Borhani S, Darvanjooghi MHK (2016) Electrospinning of cellulose nanofibers mat for laminated epoxy composite production. Fibers Polym 17:1438–1448

Jayaramudu T, Raghavendra GM, Varaprasad K, Sadiku R, Raju KM (2013) Development of novel biodegradable Au nanocomposite hydrogels based on wheat: for inactivation of bacteria. Carbohydr Polym 92:2193–2200

Kharaziha M et al (2013) PGS: gelatin nanofibrous scaffolds with tunable mechanical and structural properties for engineering cardiac tissues. Biomaterials 34:6355–6366

Lee WF, Chen YC (2004) Effect of bentonite on the physical properties and drug-release behavior of poly (AA-co-PEGMEA)/bentonite nanocomposite hydrogels for mucoadhesive. J Appl Polym Sci 91:2934–2941

Lee WF, Chen YC (2005) Effect of intercalated hydrotalcite on swelling and mechanical behavior for poly (acrylic acid-co-N-isopropylacrylamide)/hydrotalcite nanocomposite hydrogels. J Appl Polym Sci 98:1572–1580

Li A, Liu R, Wang A (2005) Preparation of starch-graft-poly (acrylamide)/attapulgite superabsorbent composite. J Appl Polym Sci 98:1351–1357

Li X, Xu S, Pen Y, Wang JJ (2008) The swelling behaviors and network parameters of cationic starch-g-acrylic acid/poly (dimethyldiallylammonium chloride) semi-interpenetrating polymer networks hydrogels. J Appl Polym Sci 110:1828–1836

Li M, Tshabalala MA, Buschle-Diller GJ (2016) Formulation and characterization of polysaccharide beads for controlled release of plant growth regulators. J Mater Sci 51:4609–4617

Ling Z et al (2019) Effects of ball milling on the structure of cotton cellulose. Cellulose 26:305–328

Nawang R, Danjaji I, Ishiaku U, Ismail H, Ishak Z (2001) Mechanical properties of sago starch-filled linear low density polyethylene (LLDPE) composites. Polym Test 20:167–172

Pachauri P, More S, Sullia S, Deshmukh SJB (2017) Purification and characterization of cellulase from a novel isolate of Trichoderma longibrachiatum. Biofuels 11:1–7

Pahlevan M, Toivakka M, Alam PJ (2018) Mechanical properties of TEMPO-oxidised bacterial cellulose-amino acid biomaterials. Eur Polym J 101:29–36

Parvathy PC, Jyothi AN (2012a) Synthesis, characterization and swelling behaviour of superabsorbent polymers from cassava starch-graft-poly (acrylamide) Starch-Stärke. Bioresour Technol 64:207–218

Parvathy PC, Jyothi AN (2012b) Synthesis, characterization and swelling behaviour of superabsorbent polymers from cassava starch-graft-poly (acrylamide). Starch-Stärke 64:207–218

Pinheiro I, Ferreira F, Souza D, Gouveia R, Lona L, Morales A, Mei LJ (2017) Mechanical, rheological and degradation properties of PBAT nanocomposites reinforced by functionalized cellulose nanocrystals. Eur Polym J 97:356–365

Reis AV, Guilherme MR, Moia TA, Mattoso LH, Muniz EC, Tambourgi EB (2008) Synthesis and characterization of a starch-modified hydrogel as potential carrier for drug delivery system. J Polym Sci, Part A: Polym Chem 46:2567–2574

Schott HJ (1992) Swelling kinetics of polymers. J Macromol Sci Part B Phys 31:1–9

Sethi J, Illikainen M, Sain M, Oksman KJ (2017) Polylactic acid/polyurethane blend reinforced with cellulose nanocrystals with semi-interpenetrating polymer network (S-IPN) structure. Eur Polym J 86:188–199

Siqueira G, Bras J, Dufresne A (2010) Cellulosic bio-nanocomposites: a review of preparation, properties and applications. Polymers 2:728–765

Sluiter A, Hames B, Ruiz R, Scarlata C, Sluiter J, Templeton D, Crocker DJ (2008) Determination of structural carbohydrates and lignin in biomass. Lab Anal Proced 1617:1–16

Spagnol C et al (2012a) Nanocomposites based on poly (acrylamide-co-acrylate) and cellulose nanowhiskers. Eur Polym J 48:454–463

Spagnol C, Rodrigues FH, Pereira AG, Fajardo AR, Rubira AF, Muniz EC (2012b) Superabsorbent hydrogel nanocomposites based on starch-g-poly (sodium acrylate) matrix filled with cellulose nanowhiskers. Cellulose 19:1225–1237

Spagnol C, Rodrigues FH, Pereira AG, Fajardo AR, Rubira AF, Muniz EC (2012c) Superabsorbent hydrogel composite made of cellulose nanofibrils and chitosan-graft-poly (acrylic acid). Carbohydr Polym 87:2038–2045

Sun X-F, Wang H-H, Jing Z-X, Mohanathas R (2013) Hemicellulose-based pH-sensitive and biodegradable hydrogel for controlled drug delivery. Carbohydr Polym 92:1357–1366

Tanan W, Panichpakdee J, Saengsuwan S (2018) Novel biodegradable hydrogel based on natural polymers: Synthesis, characterization, swelling/reswelling and biodegradability. Eur Polym J 112:678–687

Usov I et al (2015) Understanding nanocellulose chirality and structure–properties relationship at the single fibril level. Nat Commun 6:7564

Wang F, Chang PR, Zheng P, Ma X (2015) Monolithic porous rectorite/starch composites: fabrication, modification and adsorption. Appl Surf Sci 349:251–258

Wicklein B, Kocjan A, Salazar-Alvarez G, Carosio F, Camino G, Antonietti M, Bergström L (2015) Thermally insulating and fire-retardant lightweight anisotropic foams based on nanocellulose and graphene oxide. Nat Nanotechnol 10:277

Xhanari K, Syverud K, Stenius P (2011) Emulsions stabilized by microfibrillated cellulose: the effect of hydrophobization, concentration and o/w ratio. J Dispers Sci Technol 32:447–452

Xia Z, Patchan M, Maranchi J, Elisseeff J, Trexler M (2013) Determination of crosslinking density of hydrogels prepared from microcrystalline cellulose. J Appl Polym Sci 127:4537–4541

Ye L et al (2016) Physical cross-linking starch-based zwitterionic hydrogel exhibiting excellent biocompatibility, protein resistance, and biodegradability. ACS Appl Mater Interfaces 8:15710–15723

Yue Y, Han J, Han G, French AD, Qi Y, Wu Q (2016) Cellulose nanofibers reinforced sodium alginate-polyvinyl alcohol hydrogels: core-shell structure formation and property characterization. Carbohydr Polym 147:155–164

Zander NE, Dong H, Steele J, Grant JT (2014) Metal cation cross-linked nanocellulose hydrogels as tissue engineering substrates. ACS Appl Mater Interfaces 6:18502–18510

Zhao W, Jin X, Cong Y, Liu Y, Fu J (2013) Degradable natural polymer hydrogels for articular cartilage tissue engineering. J Chem Technol Biotechnol 88:327–339

Zohuriaan-Mehr M, Pourjavadi A (2003) Superabsorbent hydrogels from starch-g-PAN: effect of some reaction variables on swelling behavior. J Polym Mater 20:113